A High-Sensitivity Frequency Counter for Free-Induction-Decay Signals

Tong Gong, Ming-Rui Shu, Jiang He, Kai Liu, Yi-Ren Li, Xin-Jun Hao, Dong Sheng, Yu-Ming Wang, and Yu-Kun Feng

***Abstract*—Real-time frequency readout of time-dependent pulsed signals with a high-sensitivity are key elements in many applications using atomic devices, such as free-induction-decay (FID) atomic magnetometers. In this article, we propose a frequency measurement algorithm based on the Hilbert transform and implement such a scheme in a field-programmable gate array (FPGA)-based frequency counter. By testing pulsed exponential-decay oscillation signals in the frequency range of 10–500 kHz, this frequency counter shows a frequency sensitivity better than 100 μHz/ $\sqrt{\text{Hz}}$ at 10 Hz, with an output rate of 200 Hz. When the output rate is increased to 1000 Hz, the sensitivity remains better than 400 μHz/ $\sqrt{\text{Hz}}$ at 10 Hz. The performance on frequency sensitivity is comparable with results obtained by off-line nonlinear fitting processes. In addition, this frequency counter does not require the preknowledge of the analytic expression of the input signals. The realization of such a device paves the way for practical applications of highly sensitive FID atomic magnetometers.**

***Index Terms*—Free-induction-decay (FID) magnetometer, frequency counter, high bandwidth, high-sensitivity, Hilbert transform.**

I. Introduction

ATOMIC devices use atomic transitions for measurements of observables, and an important application of atomic devices is to measure magnetic fields [1], [2]. In recent years, atomic magnetometers have undergone rapid developments, with the sensitivity for geomagnetic measurements surpassing traditional fluxgate magnetometers [3]. The principle of these magnetometers involves converting magnetic field measurements into frequency measurements by utilizing the Larmor precession of polarized atoms in an external magnetic field [4]. For example, in a rubidium atomic magnetometer, the dynamic range within the geomagnetic field is approximately 65 000 nT, with corresponding output frequencies less than 500 kHz. Therefore, the resolution of the frequency measurement of the sensor directly affects the precision of magnetic field measurement. For atomic magnetometers working in the closed-loop mode [5], the signals are continuous oscillations with constant amplitudes. To achieve better accuracy, a pulsed working mode, which is often referred to as the free-induction-decay (FID) mode, is developed, where the amplitude of the signals is time-varying. For most geophysics applications, the detection bandwidth of the magnetometer is normally required to be as large as possible. Therefore, it is necessary to develop a high-precision and high-bandwidth frequency measurement method.

In previous research with FID magnetometers [6], the most reliable method of data analysis involves fitting the signal with a known function to obtain its frequency parameters. However, nonlinear fittings are computationally expensive. For instance, applying the Levenberg–Marquardt (LM) [7] algorithm to a segment of damped oscillating signal data with a size of 1000 points on a personal computer with a CPU of i7-6700 may requires over 0.1 s for fitting. Considering the computational speed and hardware limitations for miniaturized devices, it is desired to find frequency processing algorithms with lower computational loads. Another commonly used method relies on the pulse-counting method, including a measuring-cycle method in relatively low-frequency bands and a measuring-frequency method in relatively high-frequency bands [8]. However, such methods have intrinsic problems as quantization errors. This quantization error is practically limited by the hardware (the clock frequency and sampling rate) and the sensor bandwidth (measurement time). To address this problem, various optimization schemes have been proposed. For example, the equal-precision method reduces quantization errors during signal counting [9], while the multichannel method uses multiple counting channels to average quantization errors and enhance the measurement accuracy [10]. The multiphase clock method suppresses quantization errors by utilizing multiple reference clocks with different phases simultaneously [11]. The relative-frequency-difference method employs high-precision time-to-digital converters (TDCs) to directly measure tiny time intervals to reduce the quantization errors [12], and

Received 27 March 2025; revised 12 May 2025; accepted 18 May 2025. Date of publication 3 June 2025; date of current version 11 June 2025. This work was supported in part by the National Natural Science Foundation of China under Grant 12174372; and in part by the Scientific Instrument and Equipment Development Projects, Chinese Academy of Sciences (CAS), under Grant YJKYYQ20200043. The Associate Editor coordinating the review process was Dr. Roman Sotner. *(Corresponding author: Yu-Kun Feng.)*

Tong Gong, Jiang He, and Dong Sheng are with the Department of Precision Machinery and Precision Instrumentation, Key Laboratory of Precision Scientific Instrumentation of Anhui Higher Education Institutes, University of Science and Technology of China, Hefei 230027, China.

Ming-Rui Shu is with China Ship Research and Design Center, Wuhan 430000, China.

Kai Liu, Yi-Ren Li, Xin-Jun Hao, and Yu-Ming Wang are with the School of Earth and Space Sciences, the Deep Space Exploration Laboratory, the CAS Center for Excellence in Comparative Planetology, and the CAS Key Laboratory of Geospace Environment, University of Science and Technology of China, Hefei 230026, China (e-mail: ymwang@ustc.edu.cn).

Yu-Kun Feng is with the Department of Modern Physics, University of Science and Technology of China, Hefei 230026, China (e-mail: fyk@ustc.edu.cn).

Digital Object Identifier 10.1109/TIM.2025.3575977

the Ω-counter represents the state-of-the-art optimization of this approach, leveraging continuous timestamp registration and linear regression algorithms to extract frequency parameters with minimal computational bias [13]. However, these optimization methods either marginally improve measurement accuracy or consume excessive hardware resources. In addition, another widely used fast frequency counting method is based on spectrum analysis, such as the discrete Fourier transform [14]. The accuracy of spectral analysis depends on the sampling rate and data volume, it has been found in practice that the sensitivity based on this method is two times worse than that using the nonlinear fitting method [15].

In this article, we present a frequency measurement algorithm based on the Hilbert transform. This algorithm converts nonlinear frequency fitting to linear phase fitting without sacrificing computational accuracy, therefore simultaneously satisfies the requirements on extracting the signal oscillation frequency with a high precision and bandwidth. Schemes based on similar algorithms have been demonstrated to work in principle [16], [17]. In this work, we show that the algorithm needs to be modified for fast and precise real-time analysis applications. Furthermore, we develop a hardware system to implement this algorithm, and test its performance using pulsed signals from arbitrary function generators. The algorithm and hardware system developed in this work is not only important for atomic devices, but also can be applied in any field that requires a reliable real-time frequency extraction from pulsed oscillation signals, such as underwater acoustic signal processing [18]. The structure of the remainder of this article is as follows. Section II provides working principle of the algorithm and the hardware design, Section III presents the test results of this algorithm and hardware, and Section IV concludes this article.

II. Algorithm and Hardware Design

The Hilbert transform is widely used in signal processing, with a physical interpretation of delaying the signal by 90° in all frequency components. For a continuous-time signal $x(t)$, its Hilbert transform is denoted as $y(t) = (1/\pi)\int_{-\infty}^{\infty}(x(\tau)/(t-\tau))\mathrm{d}\tau$. If the original signal can be represented as $x(t) = \int_0^{\infty} A(\omega)\cos(\omega t + \varphi(\omega))\mathrm{d}\omega$, then its Hilbert transform results in $y(t) = \int_0^{\infty} A(\omega)\sin(\omega t+\varphi(\omega))\mathrm{d}\omega$. By using the original signal as the real part and its Hilbert transform as the imaginary part, a complex analytic signal $z(t) = x(t)+iy(t)$ can be constructed. For the signal $z(t)$, its instantaneous amplitude $A(t) = (x^2(t)+y^2(t))^{1/2}$ and instantaneous phase $\varphi(t) = \tan^{-1}(y(t)/x(t))$ at any given moment can be constructed, where the derivative of the instantaneous phase with respect to time yields the instantaneous frequency. In practice, signals are discrete, and the corresponding discrete-time Hilbert transform is represented as [19]

$$y[n] = \frac{2}{\pi}\sum \frac{x[n-k]}{k}\sin^2\left(\frac{k\pi}{2}\right), \quad k \in Z. \tag{1}$$

Suppose the discrete signal takes the form $x[n] = A[n]\sin[\omega n/f_s]$, where f_s is the sampling rate, the corresponding $y[n]$ can be expressed as

$$\begin{aligned} y[n] &= \frac{2}{\pi}\sum \frac{A[n-k]\sin[\omega(n-k)/f_s]}{k} \\ &\quad - \frac{2}{\pi}\sum \frac{A[n+k]\sin[\omega(n+k)/f_s]}{k} \\ &= \frac{2}{\pi}\sum \frac{(A[n+k]-A[n-k])\sin[\omega(n+k)/f_s]}{k} \\ &\quad - \frac{2}{\pi}\sum \frac{2A[n-k]\cos[\omega n/f_s]\sin[\omega k/f_s]}{k} \\ &\quad k = 1,3,5,\ldots \end{aligned} \tag{2}$$

Considering the practical range of signal amplitudes where $A[n] \le A_{\max}$, the expression for $y[n]$ converges for each n. Therefore, when calculating the discrete-time Hilbert transform, it is feasible to truncate at a suitable value of k to reduce computational complexity. The algorithm developed in this work, which is named as Hilbert-transform linear-regression (HT-LR) algorithm, is outlined below.

1) Utilize (1) to transform the acquired signal $x[n]$ into $y[n]$.
2) Calculate the instantaneous phase $\varphi[n] = \tan^{-1}(y[n]/x[n])$ and derive the cumulative phase $\Phi[n] = \varphi[n] + 2\pi N$ to make phase value continuous.
3) Perform a weighted linear regression fit on $\Phi(t)$ with the amplitude $z[n] = \sqrt{x[n]^2+y[n]^2}$ as the weight where $t = n/f_s$, and the extracted slope represents the oscillation frequency of the signal.

The HT-LR algorithm is implemented in a field-programmable gate array (FPGA)-based frequency counter. The hardware of this frequency counter consists of four main parts: an analog-to-digital converter (ADC) module, a communication interface, a frequency reference, and the main control chip, as shown in Fig. 1. In addition, we use a 16-bit signal generator to generate signals to test the performance of the frequency counter. In this hardware, we use 18-bit ADCs with a maximum sampling rate of 2 MSa/s. The frequency reference is an oven-controlled crystal oscillator (OCXO, 40 MHz, 50 ppb accuracy), which provides the reference clock for the frequency counter. The main control chip (ZYNQ-XC7Z020) consists of two parts: the processing system (PS) and the programmable logic (PL). The signal acquisition module is implemented on the PL side, controlling ADC signal acquisition of the test signal using a reference clock and trigger signal. The data processing module is implemented on the PS side, processing the acquired data, and mainly consists of three calculation units: discrete Hilbert transform, arctangent operation for cumulative phase calculation, and least squares linear fitting. The ZYNQ chip's PS system integrates two ARM Cortex-A9 processors, and each core can independently run different tasks. At the beginning of each acquisition processing cycle, one processor receives data from the PL side and stores it in the ZYNQ's on-chip memory (OCM). Once all data is stored, another processor retrieves the data from OCM for processing.

The hardware architecture was designed with the following considerations.

1) The ZYNQ-XC7Z020 was chosen over conventional microprocessors such as STM32 due to its hybrid architecture combining PL and dual ARM Cortex-A9 processors (PS), while general-purpose microprocessors

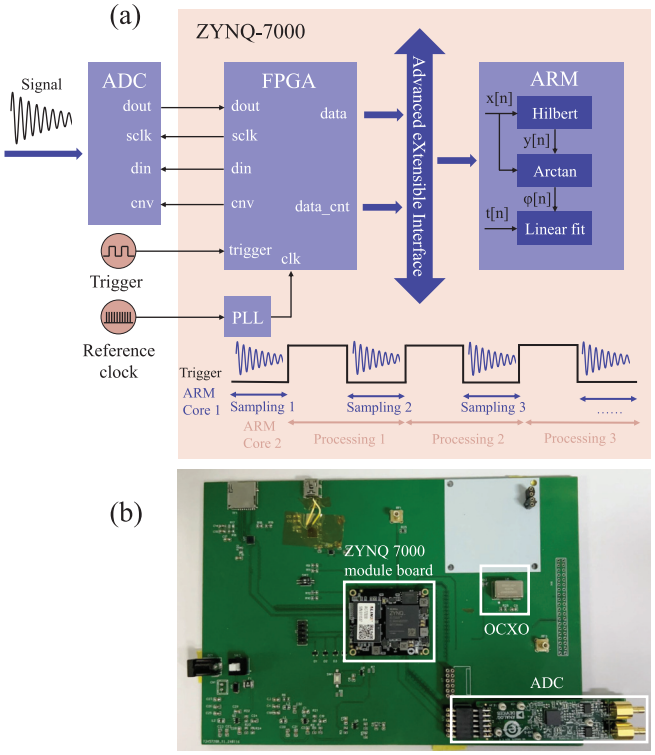

Fig. 1. (a) Schematic of the frequency counter. (b) Picture of the hardware. The circuit board includes an additional ADC interface reserved for the differential configuration of future atomic magnetometers, which was not utilized in the tests described in this work.

struggle to meet real-time processing requirements for Hilbert transforms at high sampling rate.

2) Standalone 18-bit ADCs were adopted because their simultaneous low noise and 2 MSa/s sampling rate exceed the performance of embedded ADC blocks in typical FPGA platforms.
3) Partitioning data acquisition (ARM Core 1) and signal processing (ARM Core 2) across two CPU cores provides a 50% temporal margin for computational tasks.
4) The integrated ARM cores provide a mature software ecosystem for algorithm implementation, while the FPGA enables hardware acceleration. This PS-PL co-processing framework allows seamless software-hardware co-design: complex signal processing chains can be initially prototyped on the ARM cores and later gradual migration to PL.

III. Test Results

The simulated signals take the form of damped oscillating pulses $Ae^{-t/\tau}\sin(2\pi ft)$, where signal amplitude $A = 2.5$ V, relaxation time $\tau = 2.5$ ms, f is in the range of 10–500 kHz, and the repetition rate of the signal is 200 Hz with a duty cycle of 50%. The upper frequency limit of the test signals was constrained by the ADC's maximum sampling rate, while this frequency range also corresponds to the operational bandwidth of atomic magnetometers within geomagnetic field environments. These test signals were generated by a RIGOL DG2052 function generator, which simultaneously provided a synchronized 200 Hz square-wave trigger signal. The trigger signal synchronizes ADC acquisition with the pulsed FID signal. For the application of magnetometers, it ensuring alignment between data segments and the probe/pumping cycle of the magnetometer. To be specific, the trigger signal was held at a low-level during the output of damped oscillation pulses and switched to high-level during the quiescent periods, thereby controlling the timing sequence in our frequency counter. The ADC sampling rate of the frequency counter is set to 1.53846 MSa/s (sampling interval of 650 ns). While processing data using the HT-LR algorithm, the ADC module simultaneously stores the acquired data on a memory card so that off-line nonlinear fitting of the same data can be performed for comparisons.

In practice, the infinite series sum in the discrete Hilbert transform [see (2)] needs to be truncated. This leads to the sum over k in (1) with a maximum value of K

$$y[n] = \frac{2}{\pi}\sum_{-K}^{K}\frac{x[n-k]}{k}, \quad k = \pm 1, \pm 3, \pm 5, \ldots \tag{3}$$

The precision of extracted frequency increases with the value of K, but this also increases computation time. In this work, we use the noise spectral density (NSD) value at 10 Hz (averaged between 8–12 Hz) of the extracted frequency as a main parameter to characterize the performance of the frequency counter.

Fig. 2(a) shows that the computation time for pulsed signals with a duration of 2.5 ms changes with different values of K. A horizontal line at 4.92 ms represents the time required for the same data processed by running the LM fitting function in MATLAB on a computer with a CPU of i9-13900. It can be observed that when K is less than 40, the signal processing speed of our frequency counter exceeds that of the nonlinear fitting algorithm running on a high-performance computer. Considering the hardware limitations and performance optimizations, performing nonlinear fitting on home-made data acquisition systems would require an even longer time.

To systematically characterize the measurement performance, we experimentally quantified the NSD and Δf of our frequency counter. While the mathematical theory of Hilbert-transform-based methods for FID signal processing has been rigorously established in prior works [20], this study focuses on error analysis under practical operating conditions. As shown in Fig. 2(b) and (c), as K increases, the sensitivity of the HT-LR algorithm gradually converges, so does the difference between the extracted frequencies by the HT-LR and LM algorithms. Notably, the Δf induced by the truncation parameter K constitutes the primary source of systematic error in this algorithm, though such error is one order of magnitude smaller than the typical intrinsic heading errors of the FID magnetometers used in geomagnetic fields [21]. We choose $K = 20$ in the rest of the tests, which strikes a balance between computational efficiency and precision.

The stability of crystal oscillators affects the sensitivity of frequency measurements because it determines the stability of the sampling frequency f_s. We compare the performance of the frequency counter when the time reference of the FPGA is its onboard crystal oscillator (50 ppm accuracy) with the cases

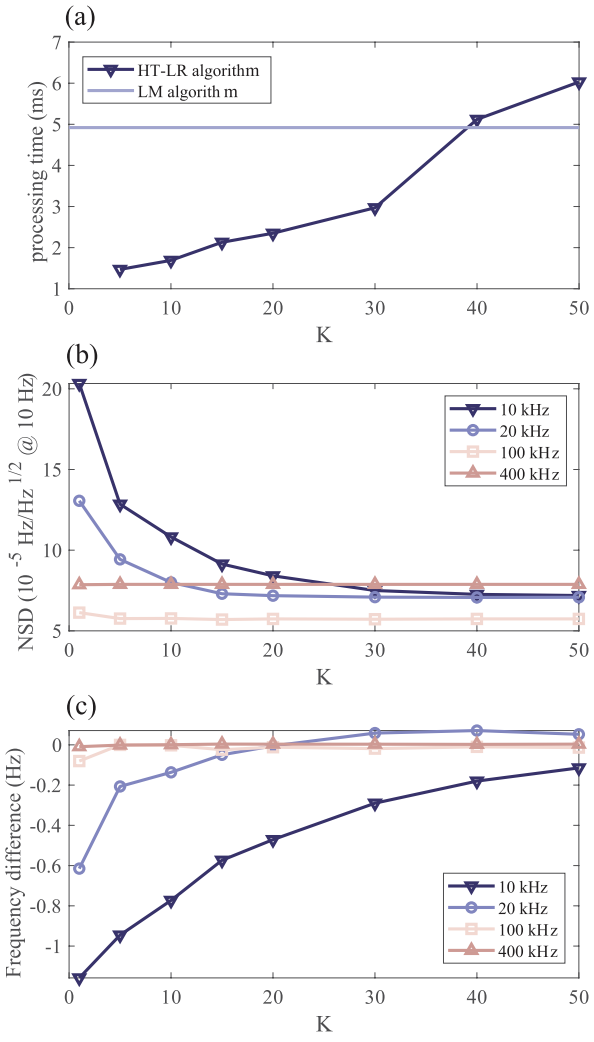

Fig. 2. (a) Computation time of the HT-LR algorithm for different K values, with the horizontal line refers to the time required for the same data processed off-line by nonlinear fitting using MATLAB on a computer with a CPU of i9-139000. To benchmark efficiency, we implemented the HT-LR algorithm in MATLAB and observed its execution time on the same workstation (i9-13900 CPU) to be merely 1/20 of that on the FPGA platform. (b) NSD value (at 10 Hz) of the frequency counter output for different K values. (c) Difference Δf between the frequency extracted with different K values with the value of extracted by off-line fitting using the LM algorithm.

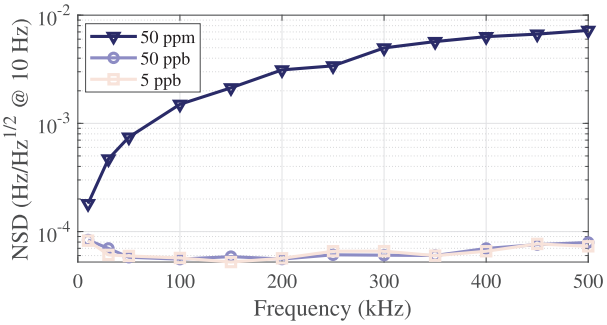

Fig. 3. Comparison of frequency counter results at different signal frequencies using oscillators with varying stability, with $K = 20$ in the HT-LR algorithm.

where the frequency references are based on two different OCXOs (50 and 5 ppb accuracy, respectively), as shown in Fig. 3. It can be concluded that for the tested signal frequency

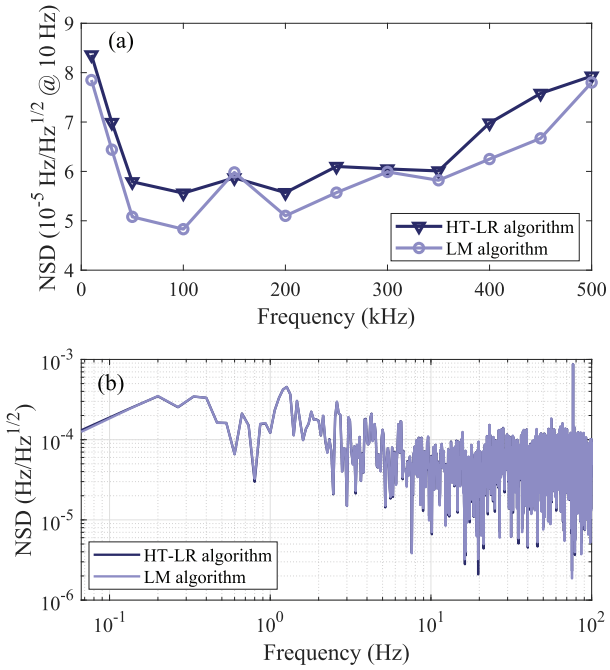

Fig. 4. (a) Comparison between the HT-LR algorithm and LM fitting at different signal frequencies, with $K = 20$ in the HT-LR algorithm. (b) NSD spectrum curve of the signal (using 200 kHz as an example).

range (10–500 kHz) and relaxation time ($\tau = 2.5$ ms), once the stability of the crystal oscillator exceeds 50 ppb, the sensitivity of the frequency counter is no longer limited by the clock stability.

Fig. 4 shows that the NSD value of real-time readout of oscillation frequencies of the pulsed input signals using our frequency counter is always better than 100 μHz/ $\sqrt{\text{Hz}}$ at 10 Hz, which is very close to the off-line fitting results using the LM algorithm. It needs to be emphasized that the increase of NSD value at both low and high frequencies is not due to the limitations from the frequency counter or LM algorithm, but rather due to the reduced signal-to-noise ratio (SNR) at these frequencies of the specific signal generator (RIGOL DG2052) used in tests. We have tried to perform the same tests using a higher precision signal generator (Zurich Instruments HDAWG), and within the frequency range of 10–500 kHz, the NSD value of the extracted frequencies from the updated device is constantly between 10 μHz/ $\sqrt{\text{Hz}}$ to 30 μHz/ $\sqrt{\text{Hz}}$ at 10 Hz.

We have also tested the influence of the detection bandwidth on the device sensitivity. Although increasing the output rate leads to a reduced processing time available for each data segment, the number of sample points per segment of data also decreases. Therefore, with $K = 20$, the total computation time remains constant for different pulse repetition rates.

Fig. 5 shows that, as the output rate increases with all other parameters kept the same in the tests, the amount of data involved in the computation decreases, leading to a corresponding decline in detection sensitivity. However, even at an output rate of 1000 Hz, the frequency sensitivity of our frequency counter remains below 400 μHz/ $\sqrt{\text{Hz}}$ at 10 Hz.

To increase the robustness of the HT-LR algorithm, we modify the linear fit part in the algorithm to a weighted fit,

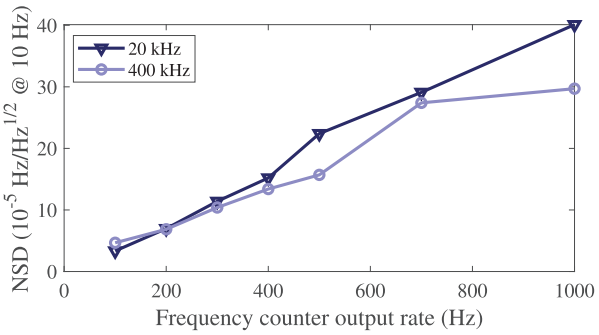

Fig. 5. NSD of the frequency counter at different output rates.

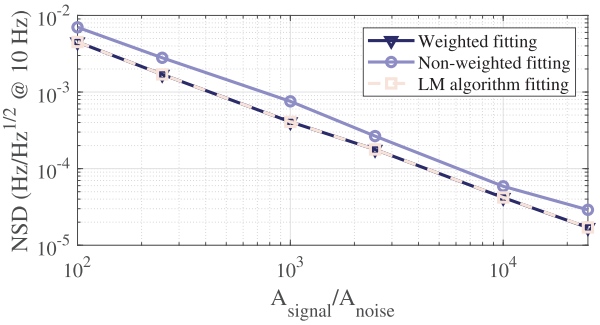

Fig. 6. NSD of 250 kHz simulated signal processed by three algorithms (gate time $T = 5$ ms).

where the weights are determined by the amplitude of the analytic function $A(t)$ mentioned in Section II. Since the SNR of the input pulsed signal decreases with time, reducing the fitting weight of the later parts of the signal can improve the quality of the fitting. We test the performance of the weighted fitting procedure using simulated data. First, we generated a batch of 3000 datasets on the computer. The data takes the form

$$V[n] = A_{\text{signal}} e^{-\frac{n}{f_s \cdot \tau}} \sin(2\pi f \cdot n/f_s) + A_{\text{noise}} \text{rand}n[n] \quad (4)$$

where $\tau = 2.5$ ms, and $f_s = 1.53846$ MSa/s. The frequency of the simulated data is set to 250 kHz, and rand$n[n]$ represents a set of standard normal distribution random numbers. We then process this data using both weighted and nonweighted HT-LR algorithms, as well as the LM fitting algorithms, comparisons of the resulted NSD are plotted in Fig. 6, and the result indicates that the weighted fitting procedure reduces the NSD by reducing the weight of low-SNR segments, with the improvement proportional to the gate time duration. Specifically, this improvement factor reaches approximately 15% at $T = 2.5$ ms, and escalates to 40% when T is extended to 5 ms. Furthermore, the results from the weighted HT-LR algorithm are almost identical to those obtained using the LM fitting algorithm. Importantly, frequency deviations caused by SNR variations exhibit no significant correlation with SNR levels and are negligible compared to aforementioned truncation-induced deviations from parameter K. This further validates the robustness of the weighted HT-LR algorithm in handling noise-contaminated signals.

According to theoretical analysis in [22], for a particular frequency f, the fundamental sensitivity limit of TDC-based Ω-counters is governed by

$$\delta f = \frac{2\sqrt{3} \cdot f^{1/2}}{T^{3/2}} \cdot \delta T \quad (5)$$

where δT denotes the TDC timing resolution. Assuming $\delta T = 20$ ps, a typical value in common commercial frequency counters, such as Keysight 53230A [23], and adopting our experimental gate time $T = 2.5$ ms, the Ω-counter's theoretical sensitivity calculates to be 20 μHz/$\sqrt{\text{Hz}}$ with the signal oscillation frequency at 250 kHz, whereas our implementation achieves an NSD between 10 to 30 μHz/$\sqrt{\text{Hz}}$ across the entire frequency band (10–500 kHz) when using the high-precision Zurich Instruments HDAWG signal generator. Notably, this comparison assumes ideal conditions for the Ω-counter: exhaustive timestamp recording for every signal cycle. We therefore conclude that the HT-LR scheme provides similar sensitivity to Ω-counters within our target frequency band, while costing less hardware resources.

IV. Conclusion

In conclusion, we have developed an algorithm based on the Hilbert transform to extract the oscillation frequency of a pulsed signal, and also implemented this algorithm in an FPGA-based frequency counter. The real-time measurement results of this device demonstrate comparable sensitivity of extracted frequency with the commonly used off-line nonlinear fitting method. With an output rate of 200 Hz, the measurement sensitivity is less than 100 μHz/$\sqrt{\text{Hz}}$ at 10 Hz, which corresponds to a background noise level of 10 fT/$\sqrt{Hz}$ for ^{87}Rb magnetometers. And even at an output rate of 1000 Hz, the measurement sensitivity is below 400 μHz/$\sqrt{\text{Hz}}$ at 10 Hz. Applications of such an algorithm and device are not limited in the field of atomic magnetometry, they can be applied to other scenarios requiring high-precision, real-time processing of pulse frequency signals. Following this work, we will focus on extending the algorithm to extract multiple frequencies and further optimizing the computational speed.

References

[1] J. Kitching, S. Knappe, and E. A. Donley, "Atomic sensors—A review," *IEEE Sensors J.*, vol. 11, no. 9, pp. 1749–1758, Sep. 2011.
[2] J. Kitching, "Chip-scale atomic devices," *Appl. Phys. Rev.*, vol. 5, no. 3, Sep. 2018, Art. no. 031302.
[3] D. Budker and M. Romalis, "Optical magnetometry," *Nature Phys.*, vol. 3, no. 4, pp. 227–234, 2007.
[4] Z. D. Grujić, P. A. Koss, G. Bison, and A. Weis, "A sensitive and accurate atomic magnetometer based on free spin precession," *Eur. Phys. J. D*, vol. 69, no. 5, pp. 1–10, May 2015.
[5] C. Abel, "Optically pumped Cs magnetometers enabling a high-sensitivity search for the neutron electric dipole moment," *Phys. Rev. A, Gen. Phys.*, vol. 101, no. 5, 2020, Art. no. 053419.
[6] D. Sheng, S. Li, N. Dural, and M. V. Romalis, "Subfemtotesla scalar atomic magnetometry using multipass cells," *Phys. Rev. Lett.*, vol. 110, no. 16, Apr. 2013, Art. no. 160802.
[7] J. J. Moré, "The Levenberg–Marquardt algorithm: Implementation and theory," in *Numerical Analysis*. Berlin, Germany: Springer, Jul. 1977.
[8] S. Keshani, N. Masoumi, H. Rahimpour, and S. Safavi-Naeini, "Digital processing for accurate frequency extraction in IFM receivers," *IEEE Trans. Instrum. Meas.*, vol. 69, no. 9, pp. 6092–6100, Sep. 2020.
[9] N. S. Kumar and D. V. R. KotiReddy, "A new method to enhance performance of digital frequency measurement and minimize the clock skew," *IEEE Sensors J.*, vol. 11, no. 10, pp. 2421–2425, Oct. 2011.

[10] H. Dong, H. Liu, J. Ge, Z. Yuan, and Z. Zhao, "A high-precision frequency measurement algorithm for FID signal of proton magnetometer," *IEEE Trans. Instrum. Meas.*, vol. 65, no. 4, pp. 898–904, Apr. 2016.
[11] J. Ge et al., "High-precision frequency measurement approach of diminishing multi-source errors for UAV-based aeromagnetic survey," *Measurement*, vol. 227, Mar. 2024, Art. no. 114312.
[12] A. Samarah and A. C. Carusone, "A digital phase-locked loop with calibrated coarse and stochastic fine TDC," *IEEE J. Solid-State Circuits*, vol. 48, no. 8, pp. 1829–1841, Aug. 2013.
[13] P. Kwiatkowski and A. Beczek, "Hardware computing module for frequency Ω-counter," *Measurement*, vol. 229, Apr. 2024, Art. no. 114404.
[14] J. C. Visschers, E. Wilson, T. Conneely, A. Mudrov, and L. Bougas, "Rapid parameter determination of discrete damped sinusoidal oscillations," *Opt. Exp.*, vol. 29, no. 5, p. 6863, Mar. 2021.
[15] K. Yi et al., "Free-induction-decay ^{4}He magnetometer using a multipass cell," *Phys. Rev. Appl.*, vol. 22, no. 1, Jul. 2024, Art. no. 014084.
[16] N. Wilson, C. Perrella, R. Anderson, A. Luiten, and P. Light, "Wide-bandwidth atomic magnetometry via instantaneous-phase retrieval," *Phys. Rev. Res.*, vol. 2, no. 1, Feb. 2020, Art. no. 013213.
[17] D. Hunter, T. E. Dyer, and E. Riis, "Accurate optically pumped magnetometer based on ramsey-style interrogation," *Opt. Lett.*, vol. 47, no. 5, p. 1230, Mar. 2022.
[18] M. Stojanovic and J. Preisig, "Underwater acoustic communication channels: Propagation models and statistical characterization," *IEEE Commun. Mag.*, vol. 47, no. 1, pp. 84–89, Jan. 2009.
[19] A. V. Oppenheim, A. S. Willsky, and S. H. Nawab, *Signals & Systems*. London, U.K.: Pearson Educación, 1997.
[20] R. Hong et al., "Systematic and statistical uncertainties of the Hilbert-transform based high-precision FID frequency extraction method," *J. Magn. Reson.*, vol. 329, Aug. 2021, Art. no. 107020.
[21] S.-Q. Liu, X.-K. Wang, X.-D. Zhang, W. Xiao, and D. Sheng, "Suppression of heading errors in bell-Bloom optically pumped free-induction-decay alkali-metal atomic magnetometers," *Phys. Rev. A, Gen. Phys.*, vol. 111, no. 2, Feb. 2025, Art. no. 023119.
[22] S. Johansson, "New frequency counting principle improves resolution," in *Proc. 20th Eur. Freq. Time Forum*, Mar. 2006, pp. 139–146.
[23] *Keysight, 53200A series RF/UNIVERSAL frequency counter/timers*, [DAtasheet]. (2021). [Online]. Available:https://www.keysight.com/us/en/assets/7018-02642/data-sheets/5990-6283.pdf

Tong Gong received the B.S. degree from East China University of Science and Technology, Shanghai, China, in 2022. He is currently pursuing the M.S. degree with the University of Science and Technology of China, Hefei, China.

His current research interests include signal processing based on the FPGA platform.

Ming-Rui Shu received the B.S. degree from Dalian Maritime University, Dalian, China, in 2020, and the M.S. degree from Tsinghua Shenzhen International Graduate School, Shenzhen, China, in 2023.

He is currently an Engineer with China Ship Research and Design Center, Wuhan, China.

Jiang He received the B.S. degree in mechanical engineering from Jilin University, Changchun, China, in 2022. He is currently pursuing the Ph.D. degree with the University of Science and Technology of China, Hefei, China.

His current research interests include miniaturized atomic magnetometers.

Kai Liu received the Ph.D. degree in geophysics from the University of Science and Technology of China, Hefei, China, in 2013.

He is currently an Engineer with the University of Science and Technology of China. His current research interests include space environmental detection, including magnetic fields and low-energy ions.

Yi-Ren Li received the Ph.D. degree from the University of Science and Technology of China, Hefei, China, in 2011.

He is now a Senior Engineer at the School of Earth and Space Sciences, University of Science and Technology of China. His current research interests include in situ detectors and its calibration systems for space plasma and magnetic fields.

Xin-Jun Hao received the B.S. degree in electronic and information engineering and the M.S. degree in information and communication engineering from Xidian University, Xi'an, China, in 2004 and 2007, respectively, and the D.Eng. degree in electronic science and technology from the University of Science and Technology of China, Hefei, China, in 2011.

His current research interests include the design of high-precision spaceborne magnetometers.

Dong Sheng received the Ph.D. degree from the University of Maryland, College Park, MD, USA, in 2011.

He is currently a Full Professor with the School of Engineering, University of Science and Technology of China, Hefei, China. His research interests include atomic devices and their applications in precision measurements.

Yu-Ming Wang received the Ph.D. degree in geophysics from the University of Science and Technology of China (USTC), Hefei, China, in 2003.

He is currently a Professor and currently serving as the Executive Dean of the School of Earth and Space Sciences, USTC. He is also the Deputy Chief Scientist of China's Planetary Exploration Project, including Tianwen-1 for Mars, Tianwen-2 for Asteroid 2016HO3, Tianwen-3 for Mars Sample Return, and Tianwen-4 for Jupiter System. His research interests include solar physics, space physics, planetary physics, and space instruments.

Dr. Wang was awarded the Xplorer Prize in 2019. He was an Editor of *Journal of Geophysical Research: Space Physics*.

Yu-Kun Feng received the B.S. and Ph.D. degrees from the University of Science and Technology of China, Hefei, China, in 2016 and 2022, respectively.

He is currently a Post-Doctoral Researcher with the School of Physics, University of Science and Technology of China. His current research interests include atomic magnetometer, co-magnetometer, and their applications.